RSC Advances

PAPER

View Article Online
View Journal | View Issue

Cite this: *RSC Adv.*, 2022, **12**, 5571

Highly luminescent $MAPbI_3$ perovskite quantum dots with a simple purification process *via* ultrasound-assisted bead milling†

Junya Enomoto, [a] Ryota Sato, [a] Masaaki Yokoyama,[a] Taisei Kimura, [a] Naoaki Oshita,[a] Kazuki Umemoto, [a] Satoshi Asakura[ab] and Akito Masuhara *[ac]

Organic–inorganic hybrid lead halide perovskite quantum dots (QDs) have various excellent optical properties, and they have drastically enhanced the field of light-emitting diode (LED) research. However, red-emissive CH_3NH_3 (MA) PbI_3 QDs have worse optical properties compared with those of green-emissive $MAPbBr_3$ QDs due to their instability under high-moisture and high-temperature conditions. Therefore, it is quite difficult to prepare $MAPbI_3$ QDs with good optical properties *via* bottom-up methods using conditions involving high temperature and high-solubility solvents. On the other hand, top-down methods for preparing $MAPbI_3$ QDs under an air atmosphere have attracted attention; however, there are issues, such as PL emission with a wide FWHM being obtained due to the wide particle-size distribution. In this research, red-emissive $MAPbI_3$ QDs were prepared *via* an ultrasound-assisted bead milling (UBM) method, and the $MAPbI_3$ QDs were purified using various carboxylate esters. As a result, we solved the issue of the wide particle-size distribution unique to top-down methods *via* purifying the $MAPbI_3$ QDs, and they achieved the following excellent optical properties: a FWHM of 44 to 48 nm and a PLQY of over 60%. Notably, a fabricated LED device with $MAPbI_3$ QDs purified using methyl acetate showed a PL peak at 738 nm and a FWHM of 49 nm, resulting in an excellent EQE value of 3.2%.

Received 7th December 2021
Accepted 31st January 2022

DOI: 10.1039/d1ra08887d

rsc.li/rsc-advances

1. Introduction

Organic–inorganic hybrid lead halide perovskite ($APbX_3$; A = CH_3NH_3 (MA) or NH_2CHNH_2 (FA); X = Cl, Br, or I) quantum dots (QDs) have attracted attention as novel light sources for use in light-emitting diodes (LEDs) owing to their high photoluminescence quantum yields (PLQYs), narrow full-width at half-maximum (FWHM) values, and tunable emission wavelengths upon adjusting the halide component.[1–5] Notably, green-emissive $MAPbBr_3$ QDs exhibit narrow emission with a FWHM of approximately 25 nm, a PLQY of over 90%, and structural stability, maintaining PL emission over 3 months.[6–8] In contrast, the optical properties of $MAPbI_3$ QDs with PL emission in the red and near-infrared regions are inferior to those of green-emissive $MAPbBr_3$ QDs. This is because $MAPbI_3$ QDs containing iodide at the X site are more sensitive to moisture, heat, and solvent polarity due to the weak ionic bonding between the inorganic PbI_2 framework and organic MA^+ cations.[3,9–11] As a result of the instability of these $MAPbI_3$ QDs, they rapidly decompose under ambient conditions,[12] which has prevented the advancement of fundamental studies and future applications. Therefore, it is significantly important to demonstrate stable $MAPbI_3$ QDs that can retain the perovskite structure under air.

To date, the synthesis of highly luminescent iodide-based (red-emissive) perovskite QDs has been achieved using two bottom-up methods: the hot injection method[13,14] and the ligand-assisted reprecipitation (LARP) method.[15,16] In hot injection, a perovskite precursor is injected into a hot solution containing the other precursor, capping ligands, and a high-boiling solvent under a nitrogen atmosphere. After injection, rapid nucleation occurs and perovskite QDs are generated. However, the synthesis of perovskite QDs using hot injection generally requires a high temperature of over 100 °C, and this high temperature decomposes $MAPbI_3$ into PbI_2, NH_3, and CH_3I.[17] On the other hand, in the LARP method, the perovskite precursors are dissolved in a polar solvent (*e.g.*, dimethyl sulfoxide or *N*,*N*-dimethylformamide), and then the precursor solution is injected into a nonpolar solvent (*e.g.*, toluene, or octane) to prepare colloidal perovskite QDs. The LARP method makes it easy to prepare perovskite QDs without requiring some conditions, such as high temperature and a nitrogen atmosphere. The challenge when using the LARP method to prepare iodide-based perovskite QDs is that the polar solvent used

[a]*Graduate School of Science and Engineering, Yamagata University, 4-3-16, Jonan, Yonezawa, Yamagata 992-8510, Japan*
[b]*Ise Chemicals Corporation, 1-3-1, Kyobashi, Chuo-ku, Tokyo, Japan*
[c]*Frontier Center for Organic Materials (FROM), Yamagata University, 4-3-16, Jonan, Yonezawa, Yamagata, 992-8510, Japan*

† Electronic supplementary information (ESI) available. See DOI: 10.1039/d1ra08887d

during synthesis strongly coordinates the PbI_2 framework, forming Pb–O bonds.[18] As a result, a perovskite structure is not formed or the structure is destroyed rapidly after formation. As another method for overcoming the problems faced when using bottom-up processes, such as the hot injection method and LARP method, the preparation of perovskite QDs *via* top-down methods has attracted attention in recent years.[19,20] A typical top-down method is the ball-milling method, which uses centrifugal force as the driving force. This method makes it possible to prepare red-emissive $MAPbI_3$ QDs without needing a high temperature of over 100 °C or polar solvent; however, there are some issues, such as a low PLQY of below 10%, a wide particle size distribution, and PL emission with a wide FWHM based on unreacted perovskite precursors.[19–21] Recently, to overcome the issues associated with previous top-down methods, an ultrasound-assisted bead milling (UBM) method was developed. In UBM, a combination of ultrasound cavitation and mechanical shear force promotes the production of perovskite QDs. In detail, through ultrasound irradiation in a reaction vessel containing the perovskite precursors, zirconia beads, and capping ligands, the intensity of collisions between zirconia beads and the precursors accelerates and, finally, the particle size was minimized on the nanoscale to improve the PLQY.[22] However, the problem of PL emission with a wide FWHM from red-emissive $MAPbI_3$ QDs has still not been solved, resulting in difficulties for LED applications. To achieve LEDs, the purification of $MAPbI_3$ QDs is significantly critical to remove the impurities such as unreacted perovskite precursors that cause PL emission with a wide FWHM. According to a previous report on the purification process, an ester solvent like ethyl acetate can be added into the as-synthesized perovskite QD dispersion, resulting in the division of perovskite QDs by particle size.[23,24] However, structurally unstable ionic $MAPbI_3$ QDs are sensitive to a high dielectric constant, so the selection of a purifying solvent for purifying $MAPbI_3$ QDs is significantly important to achieve high purity and PL emission with a narrow FWHM.

In this work, $MAPbI_3$ QDs synthesized through the UBM method were purified using various carboxylate esters due to differences in the dispersibility of $MAPbI_3$ QDs in each solvent, and narrow emission with a FWHM of 44 to 48 nm was obtained. This is because unreacted precursors and small $MAPbI_3$ QDs, which were affected by quantum confinement effects, were completely removed. As a result, we synthesized highly luminescent $MAPbI_3$ QDs with a PLQY of 63% without using high temperature or polar solvents. $MAPbI_3$ QD thin film made using $MAPbI_3$ QDs purified with methyl acetate showed a high PLQY of 48%. An LED containing $MAPbI_3$ QDs purified using methyl acetate exhibited a high external quantum efficiency (EQE) of over 3%.

2. Experimental methods

2.1. Materials

Lead(II) iodide powder (PbI_2, 99.0%), oleic acid (OAc, 90.0%), and *n*-octylamine (OAm, 99.0%) were purchased from Aldrich. Hydroiodic acid (HI, 57 wt%), toluene (99.5%), methyl acetate (98.0%), and butyl acetate (99.0%) were purchased from Wako Pure Chemical Industries. Propyl acetate (98.0%) was purchased from Tokyo Chemical Industry. Ethyl acetate (99.3%) was purchased from Kanto Chemical Co., Inc. YTZ® balls (ZrO_2 beads 50 μm in diameter) were purchased from Nikkato Co., Ltd. Poly(3,4-ethylenedioxythiophene):poly(styrenesulfonate) (PEDOT:PSS, AI4083), poly(4-butylphenyl-diphenyl-amine) (poly-TPD), and tris-[1-phenyl-1*H*-benzimidazole] (TPBi) were purchased from Clevious and American Dye Source and e-Ray Optoelectronics Technology Co., Ltd. All chemicals were used without purification.

2.2. Synthesis of methylammonium halide (MAX)

Methylammonium halide salts (MAX, X = Br and I) were synthesized following a previously reported method.[15] As an example, 7 ml of HI solution was reacted with 30 ml of methylamine solution (in methanol) in a 250 ml round-bottom flask under stirring for 2 h at 0 °C using an ice bath. Then, the solution was evaporated and the white color precipitate was collected. We purified the product *via* recrystallization using methanol and diethyl ether. The obtained product was dried under vacuum overnight.

2.3. Preparation of $MAPbX_3$ QDs

$MAPbI_3$ QDs were prepared *via* ultrasound-assisted bead milling with modifications.[22] 92.0 mg of PbI_2 (0.20 mol), 25.5 mg of MAI (0.16 mol), and 23.5 g of zirconia beads (Φ = 50 μm) were loaded into a glass vessel. 350 μl of OAc, 25 μl of OAm, and 20 ml of toluene were added into the vessel. Then, an ultrasound homogenizer was inserted into the vessel and ultrasound irradiation was carried out for 3 h. The temperature of the solution was controlled at 0 °C with a chiller to avoid undesirable heating as a result of ultrasound. After ultrasonic irradiation, the as-synthesized $MAPbI_3$ QD dispersion was centrifuged at 6000 rpm for 5 min to remove ZrO_2 beads and the supernatant was collected. $MAPbBr_3$ and $MAPb(Br/I)_3$ were prepared using the corresponding halide precursors. The moles of precursors used were fixed based on the experimental conditions for $MAPbI_3$ QDs.

2.4. Purification process of $MAPbX_3$ QDs

$MAPbX_3$ QD powder was collected *via* evaporating 4 ml of QD dispersion. The QD powder was dispersed in 300 μl of carboxylate ester (methyl, ethyl, propyl, and butyl acetate) as a purifying solvent. Then, the QDs in carboxylate ester were centrifuged at 16 500 rpm for 5 min, and the obtained precipitate was dispersed in octane.

2.5 Fabrication of $MAPbI_3$ QD LEDs

PEDOTPSS (55 wt% containing AI4083) was spin-coated onto a cleaned indium tin oxide (ITO) substrate and annealed at 150 °C for 10 min, resulting in a 40 nm-thick layer. Poly-TPD was dissolved in chlorobenzene at a concentration of 4 mg ml^{-1}. This solution was spin-coated onto the PEDOT:PSS layer and annealed at 100 °C for 10 min. Colloidal $MAPbI_3$ QDs

(10 mg ml^{-1} in octane) were spin-coated onto poly-TPD at 2000 rpm for 30 s in a N_2-filled glovebox. A TPBi (50 nm), Liq (1 nm), and Al (100 nm) anode was deposited *via* thermal evaporation under high vacuum conditions ($\sim 1 \times 10^{-5}$ Pa). The active area of the device was 2 mm^2.

2.6 Characterization

X-ray diffraction (XRD) patterns of samples were obtained based on out-plane diffraction and were measured using Rigaku Smart Lab apparatus (using Cu Kα radiation at 45 kV and 200 mA). The samples were observed using a JEOL JEM-2100F transmission electron microscope (TEM) (accelerating voltage of 200 kV). Visible absorption spectra of the samples were obtained using a JASCO V-670 spectrophotometer (detecting wavelength range of 400 to 900 nm). Photoluminescence (PL) spectra and photoluminescence quantum yields (PLQYs) of samples were obtained with a JASCO FP-8000 luminescence spectrometer (excitation wavelength of 400 nm and detection wavelength range of 400 to 900 nm). PL lifetimes were obtained using Hamamatsu C11367 Quantaurus-Tau apparatus. Electroluminescence (EL) spectra were recorded using a Hamamatsu PMA-11 photonic multichannel analyser. The current–density–voltage and luminance–voltage characteristics were measured using a Keithley 2400 source measure unit and a Minolta CS200 luminance meter, respectively.

3. Results and discussion

Colloidal $MAPbI_3$ QDs capped with OAc and OAm have been successfully synthesized *via* an UBM method with a few modifications, using MAI, PbI_2, toluene, and ZrO_2 beads. After sufficient ultrasonic irradiation, a dark red suspension was obtained. To remove impurities, including unreacted perovskite precursors and small $MAPbI_3$ QDs, a low-dielectric-constant carboxylate ester (methyl, ethyl, propyl, or butyl acetate) was added as a purifying solvent to the synthesized $MAPbI_3$ QD dispersion for purification. A schematic illustration of the perovskite QD synthesis and purification process for obtaining $MAPbI_3$ QDs is shown in Fig. 1. Table 1 shows that $MAPbI_3$ QDs were collected *via* centrifugation from all samples dispersed by different purifying solvents after the evaporation of the solvent. The differences in $MAPbI_3$ QD dispersibility are attributed to interactions between the ligands on the $MAPbI_3$ QD surface and the purifying solvent, such as methyl acetate.[3,23,25] The $MAPbI_3$ QD surface capped with OAc and OAm as ligands is hydrophobic, and the $MAPbI_3$ QDs are greatly dispersed in a solvent with a low dielectric constant and hydrophobic groups, such as toluene. On the other hand, upon using a carboxylate ester with the hydrophilic –COO– group as a dispersion solvent, interactions between the ligands on the $MAPbI_3$ QD surface and the carboxylate ester occurred as follows: some $MAPbI_3$ QDs were aggregated, and they can be easily collected *via* centrifugation. The purified $MAPbI_3$ QD dispersions show clear red emission under UV irradiation (excitation wavelength: 400 nm) (Table 1). As shown in Fig. 2, the PL spectrum of the prepared $MAPbI_3$ QDs before purification shows not only a main PL emission peak at 739 nm but also a double-shoulder PL emission peak from 600 to 700 nm, resulting a wide FWHM of 60 nm. This shoulder peak can be caused by emission from PbI_2 nanocrystals or from $MAPbI_3$ QDs with a particle size of less than 6 nm, which show quantum size effects (Fig. ES1†).[18,26] In contrast, $MAPbI_3$ QDs purified using a carboxylate ester showed narrower PL emission, with a FWHM of 44 to 48 nm, than before purification as a result of not having a PL shoulder peak attributed to impurities. The narrowing of the PL spectrum was confirmed for other types of perovskite QDs, such as $MAPbBr_3$ QDs and $MAPb(Br/I)_3$ QDs (Fig. ES2†). This implied that the purification process was adaptable to other types of perovskite QDs. However, it must be noted that the optimal purifying solvent depends on the type of perovskite QDs. Based on UV spectra, it was confirmed that the absorbance of the $MAPbI_3$ QDs gradually improved upon increasing the dielectric constant of the purifying solvent from 5.01 to 6.68 (Fig. 2b and ES3†). This implied that upon decreasing the hydrophobicity of the purifying solvent, the $MAPbI_3$ QDs were more strongly aggregated, resulting in the collection of more of them. In addition, the PLQY of the $MAPbI_3$ QDs was slightly improved from 57% to a maximum value of 63%, which implied that PbI_2 with weak PL emission was completely removed (Table ES1†).

To investigate the $MAPbI_3$ QD crystallinity and morphology, XRD patterns and TEM images were obtained (Fig. 3 and 4). From the XRD patterns, all the $MAPbI_3$ QDs showed the following diffraction peaks: 13.9° (110); 28.4° (220); 31.6° (114); 40.4° (321); and 42.9° (402), which were attributed to perovskite crystal structure.[18,27,28] Focusing on the XRD pattern of the $MAPbI_3$ QDs before purification, diffraction peaks at 12.6°, 25.9°, and 39.5° were also observed, which were attributed to the perovskite precursor PbI_2. These results clearly indicated that unreacted PbI_2 was removed from the prepared $MAPbI_3$ QD dispersion through this purification process. Diffraction peaks attributed to ZrO_2 beads and MAI, which is another perovskite precursor, were not seen (Fig. ES4†). The TEM images of the $MAPbI_3$ QDs before purification confirmed that there are two types of particles: cubic-shaped particles of about 10 nm and dot-shaped ones of less than 5 nm. On the other hand, the dot-shaped particles disappeared in all the $MAPbI_3$ QD samples after purification. Moreover, the average $MAPbI_3$ QD particle size before purification is 7.2 nm; however, after purification using methyl, ethyl, propyl, and butyl acetate, the average sizes

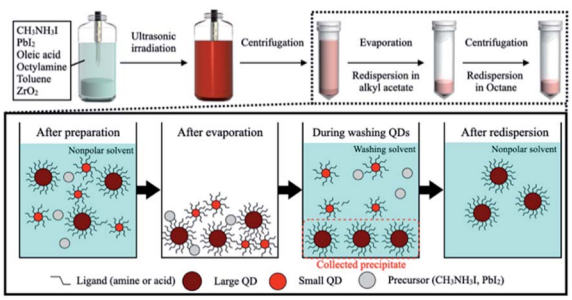

Fig. 1 A schema tic illustration of the synthesis and purification processes for obtaining $MAPbI_3$ QDs.

Table 1 The structures and dielectric constants of methyl, ethyl, propyl, and butyl acetate, and photographs of $MAPbI_3$ QDs (after centrifugation: $MAPbI_3$ QDs after dispersion in purifying solvent and centrifugation; after purification: $MAPbI_3$ QDs after the completion of the purification process)

Solvent	Structure	Dielectric constant	After centrifugation (room light)	After purification	
				Natural light	UV
Methyl acetate		6.68			
Ethyl acetate		6.02			
Propyl acetate		6.002			
Butyl acetate		5.01			

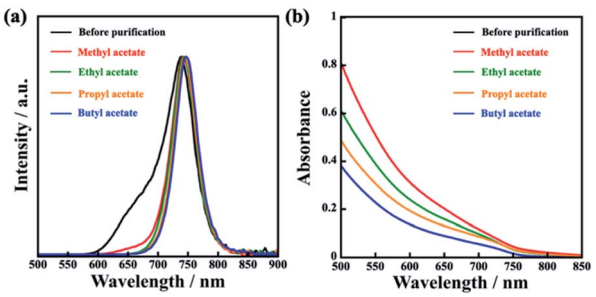

Fig. 2 (a) PL spectra and (b) absorption spectra of $MAPbI_3$ QDs before purification and $MAPbI_3$ QDs purified using methyl, ethyl, propyl, and butyl acetate.

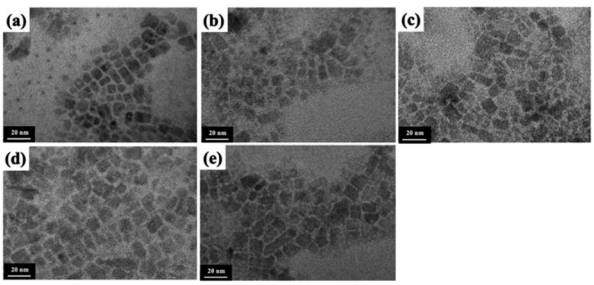

Fig. 3 TEM images of $MAPbI_3$ QDs (a) before purification and after purification with (b) methyl acetate, (c) ethyl acetate, (d) propyl acetate, and (e) butyl acetate.

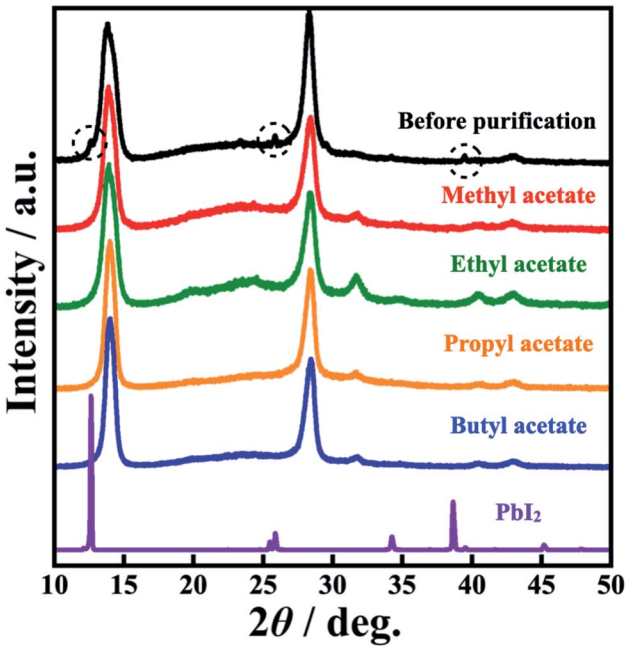

Fig. 4 XRD patterns of $MAPbI_3$ QDs before purification, $MAPbI_3$ QDs purified using methyl, ethyl, propyl, and butyl acetate, and the precursor PbI_2.

are 11.3 nm, 11.1 nm, 11.0 nm, and 11.2 nm, respectively, showing an increase in the average particle size (Fig. ES5†). This indicates that the purification of $MAPbI_3$ QDs was critical for removing the small particles. The time-resolved PL decay curves of the prepared $MAPbI_3$ QDs are shown in Fig. 5. The average PL lifetime was determined before purification to be 32.0 ns, while after purification, the lifetimes were 46.3 ns (methyl acetate), 41.8 ns (ethyl acetate), 45.6 ns (propyl acetate), and 46.1 ns (butyl acetate), showing a drastic improvement. According to previous reports,[18,29] the lifetime of $MAPbI_3$ QDs is related to the particle size, and the PL lifetime can be determined based on this. Therefore, it is possible to easily predict that the increase in the PL lifetime was related to the removal of the small-sized particles. In addition, the PLQY was slightly improved when comparing QDs before and after purification. This suggests that the number of non-luminescent sites, which are short-lived components, decreased, resulting in an increase in the PL lifetime.[30,31] From the above results, the unreacted precursors and small $MAPbI_3$ QDs causing PL emission with a wide FWHM

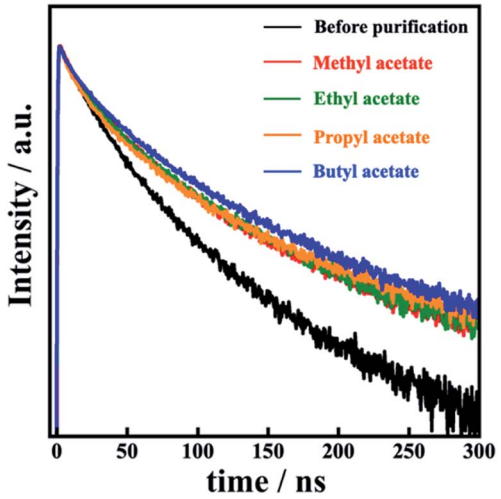

Fig. 5 Time-resolved PL decay curves of colloidal $MAPbI_3$ QDs before purification and $MAPbI_3$ QDs purified using methyl, ethyl, propyl, and butyl acetate.

were successfully removed and, notably, it was clearly proved that the best purifying solvent is methyl acetate.

Finally, in order to confirm the effectiveness of the purification process for LED applications, we demonstrated a $MAPbI_3$ QD LED with the following structure: indium tin oxide (ITO)/poly(3,4-ethylenedioxythiophene):poly(styrenesulfonate) (PEDOT:PSS; 40 nm)/poly(4-butylphenyl-diphenyl-amine) (poly-TPD; 20 nm)/$MAPbI_3$ QDs (10 nm)/tris-(1-phenyl-1*H*-benzimidazole) (TPBi; 50 nm)/lithium 8-quinolate (Liq; 1 nm)/Al (100 nm), as shown in Fig. 6a. Before evaluating the LED device characteristics, the optical properties of the $MAPbI_3$ QD thin film were clarified. The prepared $MAPbI_3$ QD thin film shows a lower PLQY of 48% than the dispersion sample, which indicates the denser packing of $MAPbI_3$ QDs on the substrate

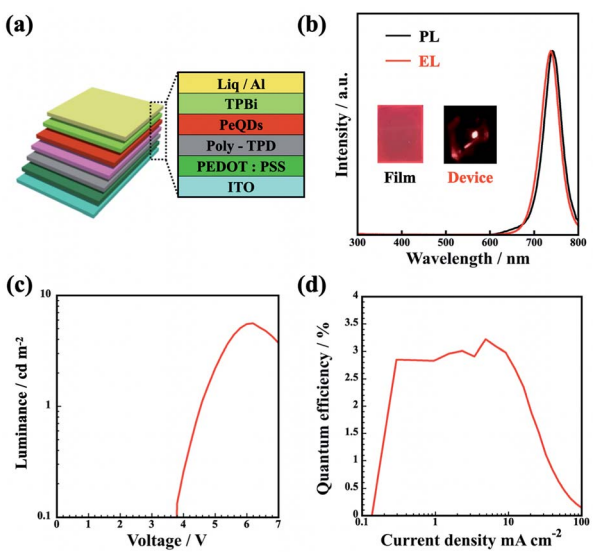

Fig. 6 (a) A schematic diagram of the device structure, (b) PL and EL spectra, (c) a luminance–voltage plot, and (d) an EQE-current density plot of an LED containing $MAPbI_3$ QDs purified using methyl acetate.

causing energy transfer to non-radiative recombination sites.[32,33] Fig. 6b shows the PL spectrum of purified $MAPbI_3$ QD thin film prepared *via* a spin-coating method and the EL spectra of the LED device with $MAPbI_3$ QDs as an emission layer. As seen in Fig. 6b, the EL spectrum of the fabricated LED has an EL peak at 738 nm and a FWHM of 49 nm, which is almost the same as the PL emission spectrum during photoexcitation (a PL peak at 741 nm and a FWHM of 48 nm). In addition, there are no differences in the EL spectrum shape at different current values (Fig. ES6a†). As shown in Fig. 6c, the turn-on voltage is 3.8 V (at 0.1 cd m^{-2}) and the maximum luminance is 5.6 cd m^{-2} at 6.2 V. The maximum EQE of the prepared LED is 3.2%, as shown in Fig. 6d; as far as we know, the EQE of these $MAPbI_3$ QDs is a new record value.[5,34,35] As a result, it can be seen that the suggested $MAPbI_3$ QD purification process utilizing the UBM method has a significant effect on the optical properties and LED device characteristics.

4. Conclusions

In summary, $MAPbI_3$ QDs with good optical properties, *e.g.*, a PLQY of over 60%, were successfully prepared *via* an UBM method, purifying the QDs using methyl acetate. This is because unreacted perovskite precursors and unsuitably sized $MAPbI_3$ QDs were removed, and the FWHM of PL emission became narrower as a result. The dielectric constant of the carboxylic acid ester used as a purifying solvent affected the absorbance (collected amount) of $MAPbI_3$ QDs, and a linear relationship was confirmed. This was caused by interactions between the alkyl ligands capping the $MAPbI_3$ QD surface and the carboxylic acid ester, especially after a decrease in the hydrophobicity of the carboxylic acid ester. In addition, the $MAPbI_3$ QD thin film based on $MAPbI_3$ QDs purified using methyl acetate showed a PLQY of 48%. A fabricated LED showed brightly luminescent EL at 738 nm with a FWHM of 49 nm, luminance of 5.6 cd m^{-2}, and maximum EQE of 3.2%, which, as far as we know, is a new record EQE for $MAPbI_3$ QDs. Interestingly, the preparation of $MAPbI_3$ QDs *via* UBM and the purification process can all be performed under air, without needing a glove box. These results indicate that the process is a simple and practical approach for optoelectronic device applications.

Conflicts of interest

There are no conflicts to declare.

Acknowledgements

This research was supported by Network Joint Research Center for Materials and Devices (20211084), Iketani Science and Technology Foundation (2020), and The Society of Iodine Science (2020).

Notes and references

1 Q. V. Le, K. Hong, H. W. Jang and S. Y. Kim, *Adv. Electron. Mater.*, 2018, **4**, 1800335.

2 P. Lu, M. Lu, H. Wang, N. Sui, Z. Shi, W. W. Yu and Y. Zhang, *InfoMat*, 2019, **1**, 430–459.
3 J. Shamsi, A. S. Urban, M. Imran, L. De Trizio and L. Manna, *Chem. Rev.*, 2019, **119**, 3296–3348.
4 C. Zhang, D. B. Kuang and W. Q. Wu, *Small Methods*, 2019, **4**, 1900662.
5 K. Ji, M. Anaya, A. Abfalterer and S. D. Stranks, *Adv. Opt. Mater.*, 2021, **9**, 2002128.
6 S. Paul and A. Samanta, *ACS Energy Lett.*, 2019, **5**, 64–69.
7 F. Krieg, S. T. Ochsenbein, S. Yakunin, S. Ten Brinck, P. Aellen, A. Suess, B. Clerc, D. Guggisberg, O. Nazarenko, Y. Shynkarenko, S. Kumar, C. J. Shih, I. Infante and M. V. Kovalenko, *ACS Energy Lett.*, 2018, **3**, 641–646.
8 Y. Tezuka, K. Umemoto, M. Takeda, Y. Takahashi, H. Ebe, J. Enomoto, S. Rodbuntum, T. Nohara, D. Fontecha, S. Asakura, T. Chiba, M. I. Furis, T. Yoshida, H. Uji-i and A. Masuhara, *Jpn. J. Appl. Phys.*, 2020, **59**, SDDC04.
9 A. M. A. Leguy, Y. Hu, M. Campoy-Quiles, M. I. Alonso, O. J. Weber, P. Azarhoosh, M. van Schilfgaarde, M. T. Weller, T. Bein, J. Nelson, P. Docampo and P. R. F. Barnes, *Chem. Mater.*, 2015, **27**, 3397–3407.
10 R. J. Sutton, G. E. Eperon, L. Miranda, E. S. Parrott, B. A. Kamino, J. B. Patel, M. T. Hörantner, M. B. Johnston, A. A. Haghighirad, D. T. Moore and H. J. Snaith, *Adv. Energy Mater.*, 2016, **6**, 1502458.
11 H. Zhao, S. Wang, M. Sun, F. Zhang, X. Li and Y. Xiao, *J. Mater. Chem. A*, 2018, **6**, 10825–10834.
12 F. Chun, B. Zhang, Y. Li, W. Li, M. Xie, X. Peng, C. Yan, Z. Chen, H. Zhang and W. Yang, *Chem. Eng. J.*, 2020, **399**, 125715.
13 L. Protesescu, S. Yakunin, M. I. Bodnarchuk, F. Krieg, R. Caputo, C. H. Hendon, R. X. Yang, A. Walsh and M. V. Kovalenko, *Nano Lett.*, 2015, **15**, 3692–3696.
14 A. Pan, B. He, X. Fan, Z. Liu, J. J. Urban, A. P. Alivisatos, L. He and Y. Liu, *ACS Nano*, 2016, **10**, 7943–7954.
15 F. Zhang, H. Zhong, C. Chen, X.-g. Wu, X. Hu, H. Huang, J. Han, B. Zou and Y. Dong, *ACS Nano*, 2015, **9**, 4533–4542.
16 Y. Tang, N. Yan, Z. Wang, H. Yuan, Y. Xin and H. Yin, *J. Alloys Compd.*, 2019, **773**, 227–233.
17 L. Ma, D. Guo, M. Li, C. Wang, Z. Zhou, X. Zhao, F. Zhang, Z. Ao and Z. Nie, *Chem. Mater.*, 2019, **31**, 8515–8522.
18 F. Zhang, S. Huang, P. Wang, X. Chen, S. Zhao, Y. Dong and H. Zhong, *Chem. Mater.*, 2017, **29**, 3793–3799.
19 L. Protesescu, S. Yakunin, O. Nazarenko, D. N. Dirin and M. V. Kovalenko, *ACS Appl. Nano Mater.*, 2018, **1**, 1300–1308.
20 S. Yun, A. Kirakosyan, S.-G. Yoon and J. Choi, *ACS Sustainable Chem. Eng.*, 2018, **6**, 3733–3738.
21 M.-G. Jeon, S. Yun, A. Kirakosyan, M. R. Sihn, S.-G. Yoon and J. Choi, *ACS Sustainable Chem. Eng.*, 2019, **7**, 19369–19374.
22 K. Umemoto, H. Ebe, R. Sato, J. Enomoto, N. Oshita, T. Kimura, T. Inose, T. Nakamura, T. Chiba, S. Asakura, H. Uji-i and A. Masuhara, *ACS Sustainable Chem. Eng.*, 2020, **8**, 16469–16476.
23 J. Li, L. Xu, T. Wang, J. Song, J. Chen, J. Xue, Y. Dong, B. Cai, Q. Shan, B. Han and H. Zeng, *Adv. Mater.*, 2017, **29**, 1603885.
24 K. Hoshi, T. Chiba, J. Sato, Y. Hayashi, Y. Takahashi, H. Ebe, S. Ohisa and J. Kido, *ACS Appl. Mater. Interfaces*, 2018, **10**, 24607–24612.
25 S. Zhou, *RSC Adv.*, 2021, **11**, 28410–28419.
26 M. Anaya, A. Rubino, T. C. Rojas, J. F. Galisteo-López, M. E. Calvo and H. Míguez, *Adv. Opt. Mater.*, 2017, **5**, 1601087.
27 C. C. Stoumpos, C. D. Malliakas and M. G. Kanatzidis, *Inorg. Chem.*, 2013, **52**, 9019–9038.
28 O. Vybornyi, S. Yakunin and M. V. Kovalenko, *Nanoscale*, 2016, **8**, 6278–6283.
29 S. B. Naghadeh, B. Luo, Y.-C. Pu, Z. Schwartz, W. R. Hollingsworth, S. A. Lindley, A. S. Brewer, A. L. Ayzner and J. Z. Zhang, *J. Phys. Chem. C*, 2019, **123**, 4610–4619.
30 C. Sun, Z. Gao, H. Liu, L. Wang, Y. Deng, P. Li, H. Li, Z.-H. Zhang, C. Fan and W. Bi, *Chem. Mater.*, 2019, **31**, 5116–5123.
31 J. Butkus, P. Vashishtha, K. Chen, J. K. Gallaher, S. K. K. Prasad, D. Z. Metin, G. Laufersky, N. Gaston, J. E. Halpert and J. M. Hodgkiss, *Chem. Mater.*, 2017, **29**, 3644–3652.
32 T. Chiba, Y. Hayashi, H. Ebe, K. Hoshi, J. Sato, S. Sato, Y.-J. Pu, S. Ohisa and J. Kido, *Nat. Photonics*, 2018, **12**, 681–687.
33 L.-P. Cheng, J.-S. Huang, Y. Shen, G.-P. Li, X.-K. Liu, W. Li, Y.-H. Wang, Y.-Q. Li, Y. Jiang, F. Gao, C.-S. Lee and J.-X. Tang, *Adv. Opt. Mater.*, 2019, **7**, 1801534.
34 Y. Hassan, O. J. Ashton, J. H. Park, G. Li, N. Sakai, B. Wenger, A. A. Haghighirad, N. K. Noel, M. H. Song, B. R. Lee, R. H. Friend and H. J. Snaith, *J. Am. Chem. Soc.*, 2019, **141**, 1269–1279.
35 P. Vashishtha, S. Bishnoi, C. H. A. Li, M. Jagadeeswararao, T. J. N. Hooper, N. Lohia, S. B. Shivarudraiah, M. S. Ansari, S. N. Sharma and J. E. Halpert, *ACS Appl. Electron. Mater.*, 2020, **2**, 3470–3490.